HHS Public Access

Author manuscript

Proc SPIE Int Soc Opt Eng. Author manuscript; available in PMC 2023 April 13.

Published in final edited form as:

Proc SPIE Int Soc Opt Eng. 2023 February ; 12465: . doi:10.1117/12.2654412.

Classification of high-risk coronary plaques using radiomic analysis of multi-energy photon-counting-detector computed tomography (PCD-CT) images

Chelsea A. S. Dunning,

Prabhakar Shantha Rajiah,

Scott S. Hsieh,

Andrea Esquivel,

Mariana Yalon,

Nikkole M. Weber,

Hao Gong,

Joel G. Fletcher,

Cynthia H. McCollough,

Shuai Leng[*]

Department of Radiology, Mayo Clinic, 200 1st St SW, Rochester, MN, USA 55905

Abstract

Coronary plaque risk classification in images acquired with photon-counting-detector (PCD) CT was performed using a radiomics-based machine learning (ML) model. With IRB approval, 19 coronary CTA patients were scanned on a PCD-CT (NAEOTOM Alpha, Siemens Healthineers) with median $CTDI_{vol}$ of 8.02 mGy. Five types of images: virtual monoenergetic images (VMIs) at 50-keV, 70-keV, and 100-keV, iodine maps, and virtual non-contrast (VNC) images were reconstructed using an iterative reconstruction algorithm (QIR), a quantitative kernel (Qr40) and 0.6-mm/0.3-mm slice thickness/increment. Atherosclerotic plaques were segmented using semi-automatic software (Research Frontier, Siemens). Segmentation confirmation and risk stratification (low- vs high-risk) were performed by a board-certified cardiac radiologist. A total of 93 radiomic features were extracted from each image using PyRadiomics (v2.2.0b1). For each feature, a t-test was performed between low- and high-risk plaques ($p<0.05$ considered significant). Two significant and non-redundant features were input into a support vector machine (SVM). A leave-one-out cross-validation strategy was adopted and the classification accuracy was computed. Fifteen low-risk and ten high-risk plaques were identified by the radiologist. A total of 18, 32, 43, 16, and 55 out of 93 features in 50-keV, 70-keV, 100-keV, iodine map, and VNC images were statistically significant. A total of 17, 19, 22, 20, and 22 out of 25 plaques were classified correctly in 50-keV, 70-keV, 100-keV, iodine map, and VNC images, respectively. A ML model using 100-keV VMIs and VNC images derived from coronary PCD-CTA best automatically differentiated low- and high-risk coronary plaques.

[*] leng.shuai@mayo.edu; phone 1 507 293 4233; www.mayo.edu/ctcic.

Keywords

photon-counting-detector; computed tomography; radiomics, machine learning; cardiac CT

1. INTRODUCTION

Cardiovascular disease (CVD) is the leading cause of death in the world and various imaging techniques have been investigated to assess patients' risk of CVD, including plaque analysis using computed tomography (CT) (1). The following four signs are what radiologists currently look for when assessing if a plaque poses a high risk of rupture causing a major adverse cardiovascular event (MACE): spotty calcification (diameter < 3 mm), low attenuation (< 30 HU), positive remodeling index of > 1.1, and the presence of a napkin-ring sign (thin fibrotic cap with a lipid core) (2, 3). Radiomics is a rapidly emerging mathematical tool which characterizes the textures and patterns of gray values within a region of interest in an image using high-order equations termed as 'radiomic features', providing objective analysis of a lesion. Radiomics outperformed conventional methods of identifying plaques with napkin-ring sign in cardiac CT (4), and its use demonstrated distinct contributions to the plaque morphology from different cardiovascular risk factors such as the aforementioned four signs, HIV infection, and history of cocaine use (5).

Photon-counting-detector CT (PCD-CT) became commercially available for cardiac imaging in 2021 (6–8). Previously, a comparison between single-energy PCD-CT and conventional CT images showed differences in high-order radiomic feature values in the myocardium, demonstrating the impact of the improved spatial resolution and noise reduction on radiomic features offered by PCD-CT technology (9). In addition to the low-energy threshold images analogous to single-energy images, PCD-CT has a multi-energy capability which allows the generation of multiple image types from the same CT angiography (CTA) acquisition such as virtual monoenergetic images (VMI), iodine maps, and virtual non-contrast (VNC) images. The different image types inherently impact contrast and texture appearance of the plaques in coronary arteries, which may in turn impact the risk assessment of MACE. Therefore, the purpose of this work is to assess the performance of coronary plaque risk stratification from multiple types of PCD-CT images using a radiomics-based machine learning (ML) model.

2. METHODS

2.1 Patient Recruitment

With Institutional Review Board approval, patients who underwent clinical coronary CTA were recruited for a same-day scan on the PCD-CT system after informed consent. The exclusion criteria encompassed patients who did not consent, did not provide authorization for use of their data for research purposes, or did not have obvious soft or mixed coronary artery plaques mentioned in the radiologist report of the clinical exam. Patients whose images had severe artifacts were also excluded, resulting in a total of 19 patients in our cohort (16 male, median age 63 (range: 30 to 78)). The plaques were classified as low-risk

or high-risk (of MACE) based on the radiologist report using plaque features such as low attenuation, spotty calcification, napkin-ring sign, and positive remodeling.

2.2 PCD-CT System and Acquisition

A clinical dual-source PCD-CT system (NAEOTOM Alpha, Siemens Healthineers, Forchheim, Germany) was used in this study. The scanner is equipped with two cadmium telluride PCD arrays and two Vectron x-ray tubes capable of 66-ms temporal resolution. The multi-energy acquisition mode (144 × 0.4 mm collimation) with energy thresholds of 20 and 65 keV was used (10). Patients were injected with 55 mL to 100 mL of iodinated contrast (Omnipaque 350, GE HealthCare, Princeton, NJ), followed by a saline chaser, and scanned with a cardiac CTA protocol: 120 kV tube potential, 0.25 s rotation time, and a median $CTDI_{vol}$ of 8.02 mGy (2.31 to 47.2 mGy) with automatic exposure control turned on (CARE Dose 4D & CARE keV, Siemens).

2.3 Image Reconstruction and Segmentation

All images were reconstructed using an offline reconstruction software (ReconCT, Siemens, v16.0.0.2449) with an iterative reconstruction algorithm (QIR) at strength 4, a medium-smooth quantitative kernel (Qr40), 1024 × 1024 matrix size, 200 mm × 200 mm field-of-view, 0.6 mm slice thickness and 0.3 mm slice increment. Five types of images were generated from the same scan for each patient: a 50 keV virtual monoenergetic image (VMI), a 70 keV VMI, a 100 keV VMI, an iodine map, and a virtual non-contrast (VNC) image. An additional 70 keV VMI mimicking clinical reference was reconstructed with the same reconstruction parameters, except with a smooth vascular kernel (Bv40) instead. The 70 keV VMIs were considered to be single-energy equivalent as the effective energy of a 120 kV beam is around 70 keV. Soft and/or mixed plaques in the native coronary arteries were segmented by two radiology fellows using semi-automatic software (Research Frontier, Siemens) on the clinical reference images, and this same segmentation (mask) was applied to the other image types. A board-certified cardiac radiologist verified plaque segmentation and risk classification in the case of difficult plaques.

2.4 Radiomic Feature Extraction and Machine Learning Model

Radiomic feature extraction was performed using PyRadiomics version 2.2.0b1 (11), an open source radiomics package based in Python 3.7.9. A total of 93 radiomic features were extracted from each segmented plaque in each image type including first order statistics and texture-based feature classes (features from shape-based classes were excluded as the same plaque mask was applied for all image types, consequently the same shape features). Texture-based feature classes included Gray Level Co-occurrence Matrix (GLCM), Gray Level Run Length Matrix (GLRLM), Gray Level Size Zone Matrix (GLSZM), Gray Level Dependence Matrix (GLDM), and Neighboring Gray Tone Difference Matrix (NGTDM). Feature definitions are listed at https://pyradiomics.readthedocs.io/. The settings for feature extraction included a bin width of 25, and resampled pixel spacing of 0.2 mm in all dimensions. The CT numbers in each image were offset such that the minimum value was equal to zero.

Manhattan plots were generated for each image type using an independent two-tailed t-test between high- and low-risk plaques for each radiomic feature, with $p<0.05$ indicating statistical significance. Features that did not meet statistical significance were discarded from analysis. The Spearman rank correlation coefficient (SRCC) was calculated among pairs of radiomic features for each image type. Two radiomic features were chosen according to the following method: the first feature with the lowest p-value, and the second feature with the next lowest p-value and a SRCC of at most a magnitude of 0.400. If the magnitude of the SRCC was greater than 0.400 between this first feature and all other significant features, then this first feature was discarded from analysis and the method proceeds using the feature with the next lowest p-value. The critical SRCC value of 0.4 was chosen based on the total number of plaques in our cohort and a 5% significance level (12). The chosen two radiomic features were input into a support vector machine (SVM, scikit-learn.org) which was trained with the radiologist report as the ground truth using a leave-one-out cross validation (LOOCV) strategy. The SVM settings were the following: a linear kernel, regularization parameter of 1, error tolerance of 1×10^{-5}, balanced class weights, and a squared hinge loss function. The accuracy was computed as the number of plaques correctly classified after each LOOCV fold and was used to assess risk stratification performance for each image type.

3. RESULTS

3.1 Plaque Images and Radiomic Results

Fifteen low-risk plaques and ten high-risk plaques were identified in the patient cohort. Example images of a patient (Figure 1) and example close-up images of a high-risk plaque in the right coronary artery and a low-risk plaque in the left anterior descending artery (Figure 2) for all types of images are shown. Different image contrasts and textures were observed among the five types of images. Blooming from iodine contrast in the lumen and calcification in the plaque was prevalent in 50 keV VMIs but not seen in 100 keV VMIs and VNC images. A total of 18, 32, 43, 16, and 55 out of 93 features in 50 keV, 70 keV, 100 keV, iodine map, and VNC images were statistically significant (Figure 3). Table 1 lists the two significant, non-redundant radiomic features that were input into the ML model.

3.2 Risk Stratification

Figure 4 shows the correlogram between the two input radiomic features into the ML model and the resulting decision boundary for a given LOOCV fold. The SVM classified 17/25 plaques correctly in the 50 keV VMIs, 19/25 correctly in the 70 keV VMIs, 20/25 correctly in the iodine maps, and 22/25 correctly in the 100 keV VMIs and VNC images.

4. CONCLUSIONS

PCD-CT systems are now approved for clinical use and capable of generating multiple image types from multi-energy data sets. A ML model using coronary CTA images from PCD-CT was developed and accurately differentiated low-risk and high-risk coronary plaques. Among the image types provided by PCD-CT, both the 100 keV VMIs and the VNC images had the highest accuracy due to a reduction in iodine and calcium

blooming in these images. Future work with larger patient cohort and direct correlation with cardiovascular outcomes is warranted, with patient recruitment ongoing. Our study using a radiomics-based ML model demonstrated the impact of PCD-CT image type on the performance of risk stratification of soft/mixed coronary plaque in coronary CTA.

ACKNOWLEDGMENTS

This study was supported in part by the National Institutes of Health under award number R01 EB028590. The content is solely the responsibility of the authors and does not necessarily represent the official views of the National Institute of Health. This study was supported in kind by Siemens Healthineers GmbH, who owns the evaluated system under the terms of a sponsored research agreement with the Mayo Clinic.

REFERENCES

1. N. C. f. H. Statistics., “Leading causes of death and numbers of deaths, by sex, race, and Hispanic origin: United States, 1980 and 2015,” (2016).
2. Conte E et al. , “Evaluation of coronary plaque characteristics with coronary computed tomography angiography in patients with non-obstructive coronary artery disease: a long-term follow-up study,” Eur Heart J Cardiovasc Imaging 18(10), 1170–1178 (2017). [PubMed: 27679600]
3. Shaw LJ et al. , “Society of Cardiovascular Computed Tomography / North American Society of Cardiovascular Imaging - Expert Consensus Document on Coronary CT Imaging of Atherosclerotic Plaque,” J Cardiovasc Comput Tomogr (2020).
4. Kolossvary M et al. , “Radiomic Features Are Superior to Conventional Quantitative Computed Tomographic Metrics to Identify Coronary Plaques With Napkin-Ring Sign,” Circ Cardiovasc Imaging 10(12), (2017).
5. Kolossvary M et al. , “Contribution of Risk Factors to the Development of Coronary Atherosclerosis as Confirmed via Coronary CT Angiography: A Longitudinal Radiomics-based Study,” *Radiology* 203179 (2021).
6. Leng S et al. , “Photon-counting Detector CT: System Design and Clinical Applications of an Emerging Technology,” Radiographics 39(3), 729–743 (2019). [PubMed: 31059394]
7. Flohr T et al. , “Photon-counting CT review,” *Phys Med* **79**(126–136 (2020).
8. Willemink MJ et al. , “Photon-counting CT: Technical Principles and Clinical Prospects,” Radiology 289(2), 293–312 (2018). [PubMed: 30179101]
9. Ayx I et al. , “Comparison Study of Myocardial Radiomics Feature Properties on Energy-Integrating and Photon-Counting Detector CT,” Diagnostics 12(5), (2022).
10. Rajendran K et al. , “First Clinical Photon-counting Detector CT System: Technical Evaluation,” *Radiology* 212579 (2021).
11. van Griethuysen JJM et al. , “Computational Radiomics System to Decode the Radiographic Phenotype,” Cancer Research 77(21), e104–e107 (2017). [PubMed: 29092951]
12. Ramsey PH, “Critical Values for Spearman’s Rank Order Correlation,” Journal of Educational Statistics 14(3), 245–253 (1989).

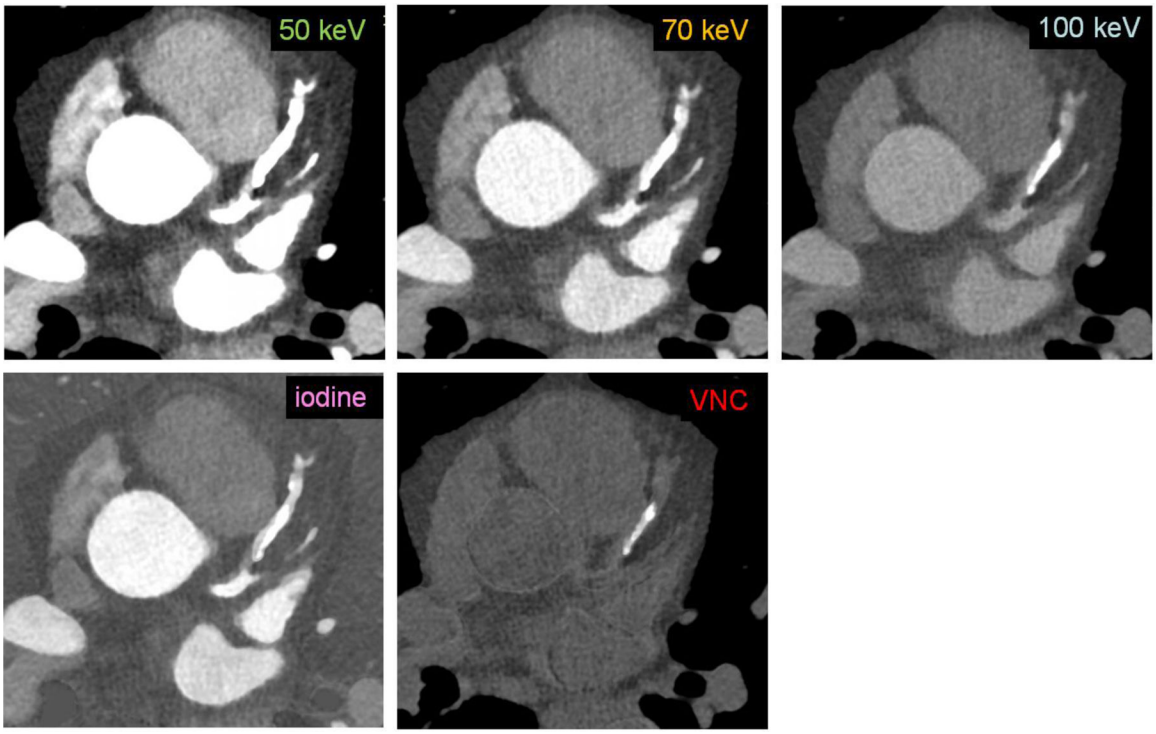

Figure 1.
Sample patient coronary CTA images from a PCD-CT (window width/window level: 900/150 HU) demonstrate the difference in appearance of calcium and iodine among the five image types (50, 70 and 100 keV VMIs, iodine, and VNC images).

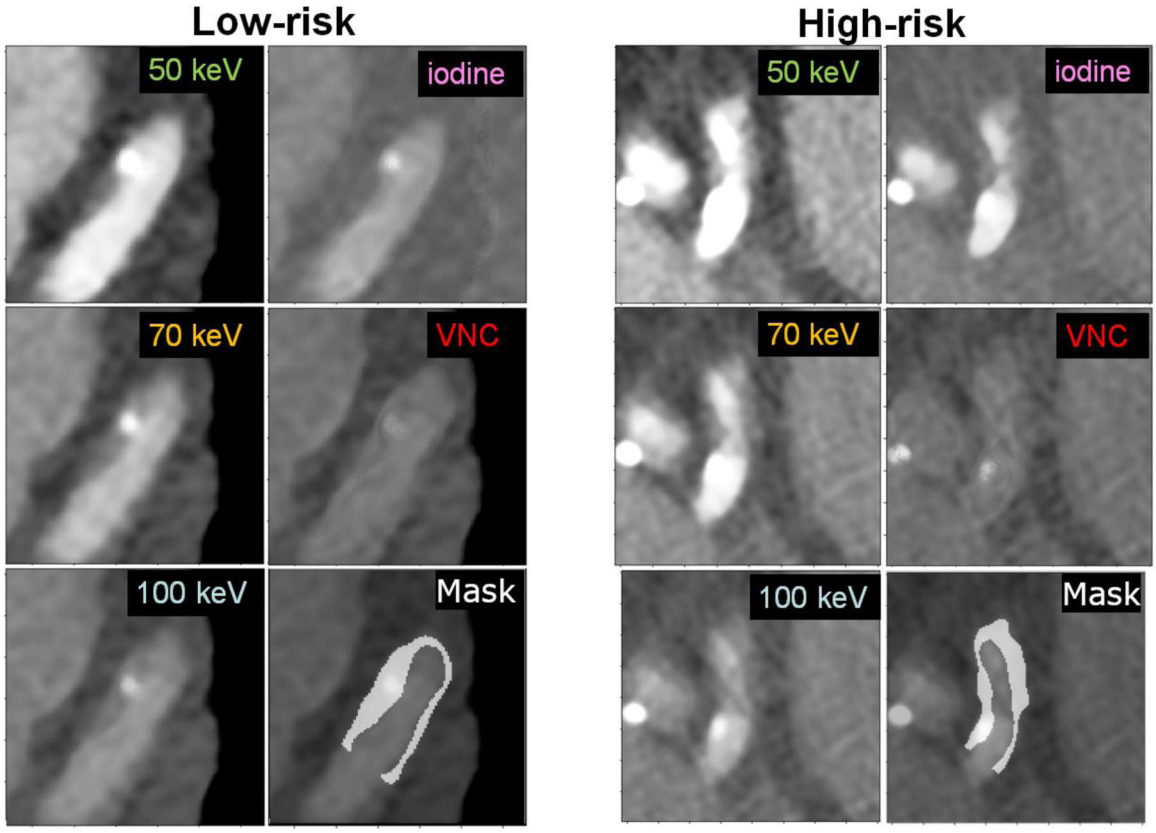

Figure 2.

Sample images (window width/window level: 900/150 HU) of two plaques from two different patients, one classified as low-risk (left) and the other high-risk (right), with their associated segmentation mask overlaid on the 100 keV VMI.

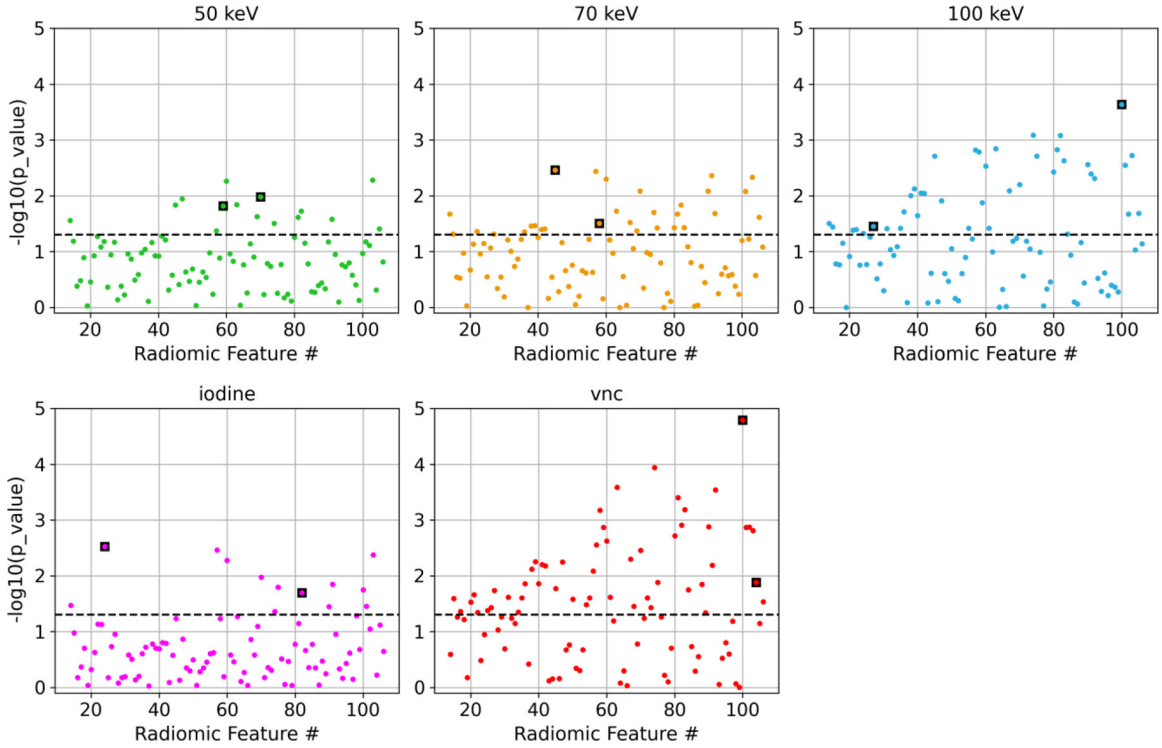

Figure 3.

Manhattan plots showing the t-test results between low- and high-risk plaques for each radiomic feature. The black dashed line represents 5% significance level. The data points outlined in a black square were chosen as input into the ML model and are listed in Table 1. The first fourteen shape-based features were not included in the analysis.

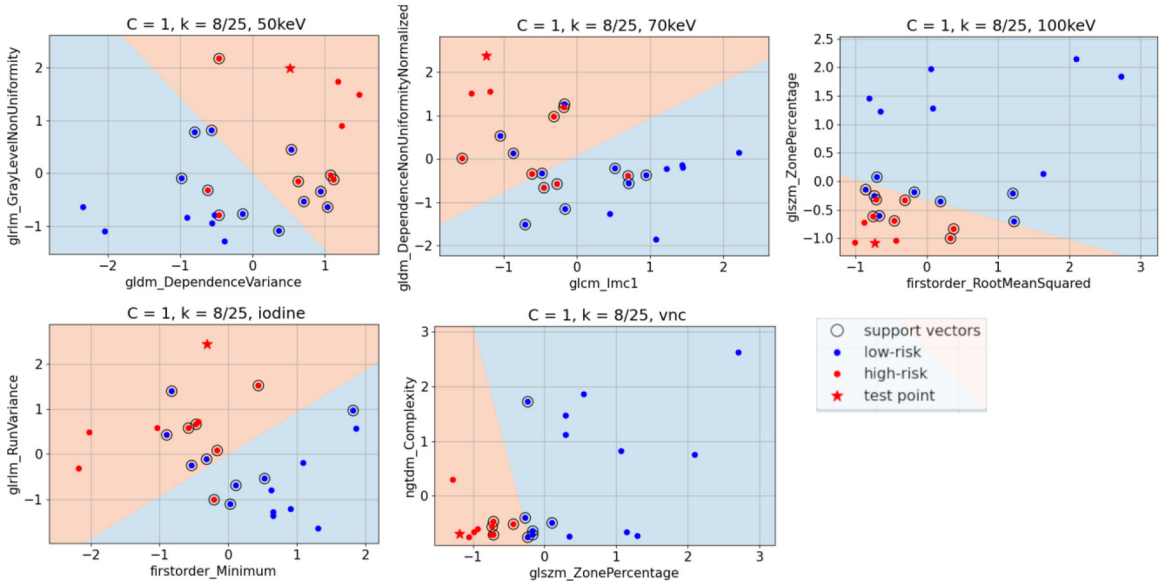

Figure 4.

Example classification of a test point (Plaque #8 out of 25, a high-risk plaque) during LOOCV for each of the five image types using the two input radiomic features into the SVM. The linear decision boundary denotes the two classification zones, high-risk (red) and low-risk (blue) of MACE.

Table 1.

The two significant, non-redundant radiomic features selected as input into the ML model for each image type. Feature definitions: https://pyradiomics.readthedocs.io/en/latest/features.html

Image type	Features for classification
50 keV VMI	GLDM_DependenceVariance GLRLM_GrayLevelNonUniformity
70 keV VMI	GLCM_Imc1 (Informational Measure of Correlation 1) GLDM_DependenceNonUniformityNormalized
100 keV VMI	firstorder_RootMeanSquared GLSZM_ZonePercentage
Iodine map	firstorder_Minimum GLRLM_RunVariance
VNC	GLSZM_ZonePercentage NGTDM_Complexity